Mixing Induced by Buoyancy-Driven Flows in Porous Media

Hamid Emami Meybodi and Hassan Hassanzadeh
Dept. of Chemical and Petroleum Engineering, Schulich School of Engineering, University of Calgary, Calgary, Alberta T2N 1N4, Canada

DOI 10.1002/aic.13891
Published online August 7, 2012 in Wiley Online Library (wileyonlinelibrary.com).

A theoretical model for fluid mixing in steady and transient buoyancy-driven flows induced by laminar natural convection in porous layers is presented. This problem follows a highly nonlinear dynamics and its accurate modeling poses numerical challenges. Based on the Taylor dispersion theory, a one-dimensional analytical model is developed for steady and transient velocity fields. To investigate steady-state mixing, a unicellular steady velocity field is established by maintaining a thermal gradient across a porous layer of finite thickness. A passive tracer is then introduced into the flow field and the mixing process is studied. In the case of transient flows, as the convective flow grows and decays with time the behavior of the dispersion coefficient is characterized by a four-parameter Weibull function. The simple analytical model developed here can recover scaling relations that have been reported in the literature to characterize the mixing process in steady and transient buoyancy-driven flows. © 2012 American Institute of Chemical Engineers *AIChE J,* 59: 1378–1389, 2013
Keywords: buoyancy-driven flows, convective mixing, dispersion, porous media, carbon dioxide sequestration

Introduction

Convective mixing is of great importance in a variety of physical frameworks, such as thermohaline circulation,[1] mixing in the Earth's mantle,[2] underground transport of pollutants and saltwater intrusion in coastal aquifers,[3] and carbon dioxide sequestration in saline aquifers.[4,5] Accurate and large-scale numerical simulations of such processes are computationally very expensive; therefore, the development of simple analytical models that can predict buoyancy-driven mixing with good accuracy is important for potential use in these applications.

Buoyancy-driven convection in porous media has received great attention during the last four decades,[6] although the porous medium analogy of the Rayleigh-Benard[7,8] convection with regard to thermal instability in a horizontal saturated porous layer was first addressed by Horton and Rogers,[9] and independently by Lapwood.[10] Depending on the physics of the problem, the buoyancy-driven flow fields can be steady or transient. Steady (frozen) flow fields have been used in the past to evaluate the mixing of passive tracers. For instance, Schmalzl and Hansen[11] numerically studied the mixing of tracers in a calculated flow field. They demonstrated that this approach could capture the Earth's mantle mixing in a detailed manner.

The development of scaling relations for the characterization of a mixing process is one of the problems of interest in many fields. Considering the fact that the majority of studies reported in the literature for mixing due to buoyancy-driven flows are based on numerical simulations, the intention of this work is the adaptation of the Taylor's theory of shear dispersion in combination with numerical simulations to derive a simple analytical mixing model that characterizes the mixing process under steady and transient flow velocity fields.

It is well-known that dispersion plays a major role in the mixing of fluids in porous media. Among different sources of dispersion, many researchers[12] have paid considerable attention to Taylor dispersion,[13,14] which in a porous medium called hydrodynamic dispersion resulted from velocity gradients. Hydrodynamic dispersion is a macroscopic outcome of the actual movements of a certain component's particles (solute) through the fluid in the porous medium. In geological media, mixing can occur by local variations in the velocity of the fluids, such as spreading a tracer during a miscible displacement.

In a laminar flow of fluids when the velocity profile varies perpendicular to the flow, a matter present in the fluid (a particle or a species) moves randomly across fast and slow streamlines by transverse diffusion. The flow of fluid and fluctuation in its velocity disperses the tracer along the direction of flow in a well-studied problem known as Taylor dispersion. Taylor[13] studied the dispersion of a passive tracer in laminar flows and obtained a simple one-dimensional (1-D) solution by assuming long-time behavior of convection-diffusion of the passive tracer in a capillary tube. Based on Taylor's dispersion theory, a shear flow can increase the effective diffusivity of a matter. Essentially, the shear acts to smooth out the concentration distribution in the direction of the flow, enhancing the rate at which it spreads in that direction under the simultaneous action of molecular diffusion and variation of the velocity.

Aris[15] considered irregularly shaped capillaries in Taylor's approach by using a method of moments. He also investigated the effects of longitudinal molecular diffusion on the dispersion process. In order that the longitudinal molecular

Correspondence concerning this article should be addressed to H. Hassanzadeh at hhassanz@ucalgary.ca.

diffusion may be negligible compared with the dispersion in Taylor's approach, it is necessary that $VR/D \gg 6.9$, where R is the tube radius, V is the mean velocity of the fluid, and D is the molecular diffusion coefficient. Later, Aris and Amundson[16] extended the Taylor dispersion theory by analyzing dispersion in packed beds. Aris[17] also studied the effects of time-periodic convection on dispersion. Horn[18] used Aris's moment scheme to extend the Taylor dispersion theory to multidimensional phase spaces, in which a basis of the generalized Taylor dispersion theory was established.

Brenner[19,20] formulated the so-called generalized Taylor dispersion theory, wherein the basic long-time, asymptotic scheme of Taylor and Aris is no longer restricted to unidirectional flows through conduits of uniform cross sections. Later, he extended the generalized theory by including the coupling phenomena that arises from the fact that the global transport process may be driven by local gradient and vice versa.[21] The generalized Taylor dispersion theory has paved the way for studying flow and dispersion phenomena in porous media, chromatographic separation processes, and heat transfer in cellular media, to mention just a few examples of the broad class of non-unidirectional transport phenomena. A comprehensive review on the Taylor's theory of shear dispersion has been presented by Young and Jones.[22]

Woods and Linz[23] investigated the transport of passive tracers governed by convection in a tilted fracture. They proposed a dispersion coefficient of a passive tracer transported by thermal convective flows as a function of Rayleigh number based on shear dispersion. In another study, Linz and Woods[24] modified the Taylor's dispersion theory and showed that dispersion not only enhances the ordinary diffusion of a tracer in tilted porous media but also dominates the spreading of passive particles in the flow field. Many other extensions of the Taylor dispersion theory have been developed and applied to a vast array of practical problems, including transport in porous media[25,26] as well as open fluids.[27–33]

We recently developed a mixing model for *steady* velocity field based on shear flow dispersion theory, in which the velocity field was obtained analytically. Using the analytically derived velocity field, longitudinal and transverse dispersion coefficients for a unicellular convective system were evaluated and eventually the mixing process was characterized.[34] In the present study, we adopt the framework of the Taylor dispersion theory combined with the velocity fields obtained from high-resolution numerical simulations to study mixing induced by *steady* and *transient* buoyancy-driven flows. This approach assists us to quantify the mixing process in the form of dispersion. In our analysis, the system is initially stagnant (no advective flow) and the dispersion is only due to the existence of velocity gradient caused by natural convection. We present a 1-D analytical model that predicts mixing of diffusing species (matter) for both steady and transient convective systems. A numerical model is also developed to evaluate mixing. Results of direct numerical modeling are then compared with those of the 1-D analytical model.

The outline for the remainder of this article is as follows. First a definition of the problem and the governing equations will be presented. Then, based on the Taylor dispersion theory, a simple 1-D analytical model will be described that models total mixing in steady-state and transient (decaying) buoyancy-driven flows. Quantitative comparisons between direct high-resolution numerical simulations and the theoretical analysis will be then made by the examination of average mixing over time, and at the end conclusions will be given.

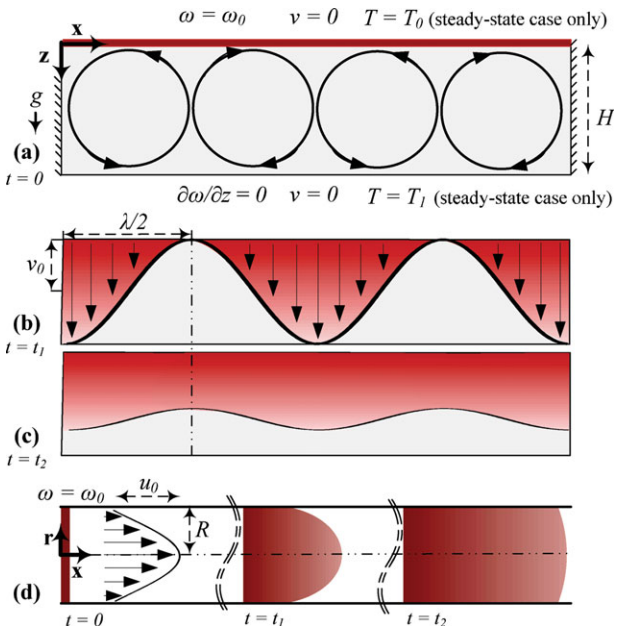

Figure 1. (a) Schematic representation of the convection cells and geometry of the domain with imposed boundary conditions.

(b) An example of velocity profile (arrows) corresponding to the convection cells in part (a), and the concentration field (shaded areas) of the diffusing species resulted from buoyancy-driven flow. (c) Concentration distribution after applying Taylor's second limiting condition on concentration profile in part (b). (d) Schematic representation of the Taylor dispersion theory in a tube. [Color figure can be viewed in the online issue, which is available at wileyonlinelibrary.com.]

Problem Statement

We considered a two-dimensional (2-D) fluid-saturated porous layer of finite thickness H and finite length L that is impervious to flow from the top and bottom as well as its sides. Schematic of the porous layer is shown in Figure 1a. The porous layer is modeled as a homogeneous and isotropic medium. The flow model consists of the incompressible flow assumption coupled with the Boussinesq approximation.[35] Accordingly, the flow equation can be expressed by[36]

$$\nabla \cdot \mathbf{v} = 0 \tag{1}$$

and fluid velocity is described by Darcy's law[37]

$$\mathbf{v} = -\frac{k}{\mu}(\nabla p - \rho g \mathbf{e}_z) \tag{2}$$

where k is the permeability, μ is the fluid viscosity, ρ is the fluid density, g is the gravity acceleration, $\mathbf{e}_z$ is the unit vector pointing downward, and $\mathbf{v} = [u,v]$ with u as the horizontal component of velocity and v as the vertical component of velocity.

Transient case

In the case of transient mixing, the top boundary is exposed to a constant concentration of a diffusing species (ω_0) and is closed from the bottom. Diffusion of the species into the resident fluid creates a diffusive boundary layer, which grows with time. As the mixed fluid density is greater than the resident fluid, the diffusive boundary layer may

become gravitationally unstable under some circumstances. The evolution of instabilities is manifested with the growth of fingers of dense fluid penetrating into the light fluid. Therefore, the system develops buoyancy-driven mixing by generating convection cells that first grow and then decay with time, due to the closed boundary at the bottom.

An ideal schematic of cells generated by laminar natural convection at a particular time and the corresponding velocity profile are shown in Figures 1a and 1b, respectively. For such a system, the conservation equation for mass is[37]

$$\rho\phi\frac{\partial\omega}{\partial t} = \nabla\cdot(\rho\phi D\nabla\omega - \rho\omega\mathbf{v}) \tag{3}$$

where ϕ is the volumetric fluid content (porosity), t is the time, ω is the diffusing species mass fraction, and D is the effective molecular diffusion coefficient. In the transient problem, the mixture density is a function of the mass fraction as given by

$$\rho = \rho_0(1+\beta_\omega\omega) \tag{4}$$

where ρ_0 is the density of the resident fluid at $t = 0$ and β_ω is considered constant because it does not vary significantly over the range of concentration exists in the problem under consideration. Based on Eq. 4, in the transient case density differences arise only owing to concentration.

In the transient case, we solve the continuity equation and the convection-diffusion equations given by Eqs. 1 and 3, respectively. However, for the steady case, we use a thermally driven natural convection to establish a steady velocity field and investigate the mixing of a passive tracer in the generated field. Therefore, for the steady case, we need to solve for the temperature field, in addition to the velocity and concentration fields, and the details of this will be described below.

Steady-state case

To determine the role of steady-state convective mixing, one needs to decouple the velocity and concentration fields by maintaining a frozen flow field. In this case, convection cells can be generated by thermal convection, as shown in Figure 1a. More precisely, the resident fluid is subjected to a destabilizing vertical temperature gradient by maintaining the top and bottom boundaries at different temperatures, T_0 and T_1 where $T_1 > T_0$. The subsequent flow is driven only by the effect of thermal buoyancy. In this case, the temperature field can be determined by the energy balance as given by[37]

$$\sigma\frac{\partial T}{\partial t} = \nabla\cdot(\alpha\nabla T - T\mathbf{v}) \tag{5a}$$

$$\sigma = \phi + (1-\phi)\frac{(\rho c)_s}{(\rho c)_f} \tag{5b}$$

$$\alpha = \frac{\phi\kappa_f + (1-\phi)\kappa_s}{(\rho c)_f} \tag{5c}$$

where T is the temperature, c_s and c_f are the specific heat capacities of the solid matrix and fluid mixture, respectively, and κ_s and κ_f are the thermal conductivity of the solid matrix and fluid mixture, respectively.

In the steady-state problem, the mixture density is a function of the temperature by

$$\rho = \rho_0(1-\beta_T(T-T_0)) \tag{6}$$

where β_T is considered constant due to the fact that it does not vary significantly over the range of temperature exists in the problem under consideration. Based on Eq. 6, in the steady-state case density differences arise only owing to temperature.

After the establishment of natural convection induced by the thermal gradients, the system reaches its steady-state condition; and, the velocity of the convection cells becomes invariant with time. A passive tracer is then introduced on top of the domain. As the flow and concentration fields are decoupled ($\beta_\omega = 0$), the mixing of the passive tracer can be described by imposing the steady thermal flow field and Eq. 3. This allows for the determination of the mixing of the passive tracer in the resident fluid by a thermal convective current until the domain is saturated with the tracer.

Numerical setup

Two different sets of equations are solved for the evaluation of the buoyancy-driven mixing. The first set includes Eqs. 1–4 for the determination of the mixing in a transient velocity field. The second set of equations, which includes Eqs. 1–6 with $\beta_\omega = 0$, are solved for the determination of the mixing in a steady-state flow field.

The governing equations are discretized using a finite difference formulation in a block-centered Cartesian grid system and have been reported in the literature for solving buoyancy-driven flow in porous medium.[38,39] An implicit scheme is used to discretize the flow equation (Eq. 1), while the transport equations (Eqs. 3 and 5) are discretized explicitly. To control the oscillations due to temporal and spatial discretizations, the grid Courant number (Cr_j) and the grid Peclet number (Pe_j) are checked to meet the following criteria[40,41]

$$Cr_j = \frac{v_j\Delta t}{\phi\Delta l_j} \le 1 \tag{7a}$$

$$Pe_j = \max\left(Pe_j^\omega, Pe_j^T\right) \le 2, \text{ in which}$$

$$Pe_j^\omega = \frac{v_j\Delta l_j}{D\phi} \text{ and } Pe_j^T = \frac{v_j\Delta l_j}{\alpha} \tag{7b}$$

$$Cr_j \le \frac{Pe_j}{2} \tag{7c}$$

where subscript j refers to the grid block index, Δl is the grid block size (Δx or Δz), v is the velocity (u or v) and Pe_j^ω and Pe_j^T are the solutal and thermal grid Peclet numbers, respectively.

In addition to these criteria, it has been suggested that for buoyancy-driven flows, the following condition should also be satisfied[42]

$$Ra_j = \max\left(Ra_j^\omega, Ra_j^T\right) \le 7, \text{ in which}$$

$$Ra_j^\omega = \frac{kg\Delta\rho_\omega\Delta z_j}{D\phi\mu} \text{ and } Ra_j^T = \frac{kg\Delta\rho_T\Delta z_j}{\alpha\mu} \tag{8}$$

where $\Delta\rho_\omega = \beta_\omega\rho_0\omega_0$ is the solutal density difference, $\Delta\rho_T = \beta_T\rho_0(T_1 - T_0)$ is the thermal density difference and Ra_j^ω and Ra_j^T are the solutal and thermal grid Rayleigh numbers, respectively.

The overall Nusselt number (the dimensionless rate of heat flux at the top and bottom boundaries) and the Sherwood number (the dimensionless rate of mass flux at the top

boundary) are defined with reference to the respective pure conduction and diffusion rates, respectively[43]

$$Nu = \frac{q^T_{\text{Cond+Conv}}}{q^T_{\text{Cond}}}, \quad q^T = -\int_0^L \left.\frac{\partial T}{\partial z}\right|_{z=0,H} dx \tag{9}$$

$$Sh = \frac{q^\omega_{\text{Diff+Conv}}}{q^\omega_{\text{Diff}}}, \quad q^\omega = -\int_0^L \left.\frac{\partial \omega}{\partial z}\right|_{z=0} dx \tag{10}$$

In the following, we use the Taylor dispersion theory to derive the 1-D mixing model for steady and transient buoyancy-driven velocity fields.

Analytical Model

The focus of the analytical modeling in this study is on the relationship between the concentration field caused by the interaction between the flow and imposed concentration difference (i.e., $\omega_0 - \omega$, where ω varies between 0 and ω_0) for both steady-state and transient convective mixing systems.

According to the system described in Figure 1, the dimensionless form of the conservation equation for mass (Eq. 3) in two-dimensions is given by

$$\frac{\partial^2 \hat{\omega}}{\partial \hat{x}^2} + \frac{\partial^2 \hat{\omega}}{\partial \hat{z}^2} = \frac{\partial \hat{\omega}}{\partial \hat{t}} + Ra\left(\hat{u}\frac{\partial \hat{\omega}}{\partial \hat{x}} + \hat{v}\frac{\partial \hat{\omega}}{\partial \hat{z}}\right) \tag{11}$$

where $Ra = k\Delta\rho g H/D\phi\mu$ and is the Rayleigh number.

From Figure 1b, it is assumed that, for a buoyancy-driven convective current, the distribution of vertical component of velocities obeys the relationship of

$$\hat{v} = \hat{v}_0 \cos[\hat{\alpha}\hat{x}] \tag{12}$$

where (^) indicates dimensionless variables, given in the following

$$\hat{x} = \frac{x}{H}, \quad \hat{z} = \frac{z}{H}, \quad \hat{t} = \frac{Dt}{H^2} \tag{13a}$$

$$\hat{v} = \frac{v}{v_{\max}}, \quad \hat{v}_0 = \frac{v_0}{v_{\max}}, \quad v_{\max} = \frac{k\Delta\rho g}{\mu} \tag{13b}$$

$$\hat{\alpha} = \alpha H, \quad \alpha = \frac{2\pi}{\lambda} \tag{13c}$$

$$\hat{\omega} = \frac{\omega}{\omega_0}, \quad \hat{K} = \frac{K}{D} \tag{13d}$$

where K is the effective dispersion coefficient, v_0 is the amplitude of the vertical component of velocity, α is the wave number, and λ is the wavelength. Later, it can be seen that the assumption presented in Eq. 12 agrees well with the numerical results.

Combining Eq. 11 with Eq. 12 results in

$$\frac{\partial^2 \hat{\omega}}{\partial \hat{x}^2} + \frac{\partial^2 \hat{\omega}}{\partial \hat{z}^2} = \frac{\partial \hat{\omega}}{\partial \hat{t}} + Ra\left(\hat{u}\frac{\partial \hat{\omega}}{\partial \hat{x}} + \hat{v}_0 \cos[\hat{\alpha}\hat{x}]\frac{\partial \hat{\omega}}{\partial \hat{z}}\right) \tag{14}$$

Assuming that the diffusive flux is much less than the convective flux in the z-direction and neglecting the convective flux in the x-direction with respect to diffusive flux, Eq. 14 becomes

$$\frac{\partial^2 \hat{\omega}}{\partial \hat{x}^2} = \frac{\partial \hat{\omega}}{\partial \hat{t}} + Ra\hat{v}_0 \cos[\hat{\alpha}\hat{x}]\frac{\partial \hat{\omega}}{\partial \hat{z}} \tag{15}$$

As shown in Figure 1, based on Taylor's dispersion theory,[13] the following limiting conditions are considered to find an approximate solution of Eq. 15: (a) The changes in concentration due to convection in vertical direction occur in a much shorter time than changes due to diffusion, so that diffusion may be neglected in z-direction. (b) The time for diffusion in x-direction to smooth the concentration profile in z-direction (time of decay) is much shorter than the time necessary for appreciable effects to appear due to transport by convection in z-direction. This situation corresponds to time t_2 in Figure 1c.

To find the situation under which condition (b) may be expected to be valid, it is necessary to calculate how rapidly a concentration profile that is a function of $\hat{x}$ deforms into a uniform concentration. The time in which the variations of concentration in x-direction decay to $1/e$ (diffusion time $1/\gamma_n^2$ in Eq. 18 is equal to time $\hat{t}$) of its initial values is the time scale for which this assumption can be made.[13] The governing differential equation in this case is

$$\frac{\partial^2 \hat{\omega}}{\partial \hat{x}^2} = \frac{\partial \hat{\omega}}{\partial \hat{t}} \tag{16}$$

and the related initial and boundary conditions are

$$\hat{\omega}(\hat{x}, 0) = 0, \quad \hat{\omega}(0, \hat{t}) = 1, \quad \frac{\partial \hat{\omega}}{\partial \hat{x}}\left(\frac{\lambda}{2H}, \hat{t}\right) = 0 \tag{17}$$

The solution to Eq. 16 subjected to Eq. 17 can be obtained using the separation of variable method,[44] as given by

$$\hat{\omega}(\hat{x}, \hat{t}) = 1 - 4\pi \sum_{n=1}^{\infty} \frac{1}{n} \exp\left[-\gamma_n^2 \hat{t}\right] \sin[\gamma_n \hat{x}] \tag{18}$$

where γ_n are eigenvalues of $\cos[\gamma_n \hat{x}]$ with $\gamma_n = n\pi H/\lambda$.

The minimum time in which the concentration variations reach $1/e$ corresponds to a lower value of $n = 1$ (i.e., to find the first eigenvalue) and it is given by

$$\hat{t}_{\text{Diff(decay)}} = \left(\frac{\lambda}{\pi H}\right)^2 \tag{19}$$

On the other hand

$$\hat{t}_{\text{Conv}} = \frac{D\phi}{H v_0} \tag{20}$$

Knowing that $\hat{t}_{\text{Conv}} \gg \hat{t}_{\text{Diff(decay)}}$ results in

$$\frac{Ra\hat{v}_0}{\hat{\alpha}^2} << \frac{1}{4} \tag{21}$$

Equation 21 demonstrates that Taylor's second limiting condition is applicable for cases with low Rayleigh numbers or high wave numbers. As our problem of interest follows a highly nonlinear dynamics, the condition obtained here needs to be modified. Therefore, we express the condition (Eq. 21) by $\delta\, Ra\hat{v}_0/\hat{\alpha}^2 << 0.25$, where δ is a constant that modifies the condition, to take into account the inherent dissimilarity of the Taylor's physical problem (Figure 1d) and buoyancy-driven mixing in porous media (Figures 1a–c). This constant (δ) is determined from direct numerical simulations of the mixing process, which will be discussed later.

As diffusion in the vertical direction has been neglected, the total transfer of matter in the z-direction is due to convection. Based on Taylor's second limiting condition, diffusion has nearly homogenized concentrations in the x-direction. Given that the mean vertical velocity across horizontal planes at constant $\hat{z}$ is zero ($\hat{z_1} = \hat{z} + V\hat{t}$, where here $V = 0$ then $\hat{z_1} = \hat{z}$), the transfer of matter across horizontal planes depends only on small variations of concentrations in x-direction. In the case where concentration variation is independent of $\hat{z_1}$, the variation in x-direction decays rapidly; as a result, concentration variations with time can be neglected ($\partial\hat{\omega}/\partial\hat{\boldsymbol{t}} = \mathbf{0}$) and $\partial\hat{\omega}/\partial\hat{\boldsymbol{z}}_{\mathbf{1}}$ ($\partial\hat{\omega}/\partial\hat{z}$) becomes constant along the finger. Therefore, small concentration variations in x-direction can be obtained by

$$\frac{\partial^2\hat{\omega}}{\partial\hat{x}^2} = Ra\hat{v}_0\cos[\hat{\alpha}\hat{x}]\frac{\partial\hat{\omega}}{\partial\hat{z}_1} \tag{22}$$

with the boundary condition of

$$\frac{\partial\hat{\omega}}{\partial\hat{x}}\left(\frac{\lambda}{2H},\hat{t}\right) = 0 \tag{23}$$

The solution to Eq. 22 subjected to Eq. 23 is

$$\hat{\omega} = w - \frac{Ra\hat{v}_0}{\hat{\alpha}^2}\cos[\hat{\alpha}\hat{x}]\frac{\partial\hat{\omega}}{\partial\hat{z}_1} \tag{24}$$

where w is a constant.

The rate of mass transfer across the horizontal plane $\hat{z_1}$ is

$$Q = \int_0^{\lambda/2H}\hat{v}\hat{\omega}d\hat{x} = -\left(\frac{Ra\hat{v}_0}{\hat{\alpha}}\right)^2\frac{\lambda}{4H}\frac{\partial\hat{\omega}}{\partial\hat{z}_1} \tag{25}$$

Under Taylor's second limiting condition, the longitudinal variations in $\hat{\omega}$ ($\partial\hat{\omega}/\partial\hat{z}_1$) are assumed to be constant and indistinguishable from the mean concentration ($\partial\hat{\omega}_m/\partial\hat{z}_1$); therefore

$$Q = -0.5\left(\frac{Ra\hat{v}_0}{\hat{\alpha}}\right)^2\frac{\lambda}{2H}\frac{\partial\hat{\omega}_m}{\partial\hat{z}_1} \tag{26}$$

In comparison with Fick's law of diffusion, $Q = -\hat{K}A(\partial\hat{\omega}_m/\partial\hat{z}_1) = -\hat{K}(\lambda/2H)(\partial\hat{\omega}_m/\partial\hat{z}_1)$ gives[36]

$$\hat{K}_{\text{Taylor}} = 0.5\left(\frac{Ra\hat{v}_0}{\hat{\alpha}}\right)^2 \tag{27}$$

where $\hat{K}_{\text{Taylor}}$ is the dispersion coefficient obtained based on the Taylor dispersion theory. This dispersion coefficient is applicable to conditions where the criterion given by Eq. 21 holds. To consider the deviations from the Taylor's limiting condition (b), the dispersion coefficient (Eq. 27) needs to be modified. Using $\delta\, Ra\hat{v}_0/\hat{\alpha}^2 << 0.25$, it can be shown that the modified dispersion coefficient can be expressed by $\hat{K} = \delta\hat{K}_{\text{Taylor}}$.

Using the conservation of mass, $Q\Delta\hat{t}|_{\hat{z}_1} - Q\Delta\hat{t}|_{\hat{z}_1+\Delta\hat{z}_1} = \hat{\omega}_m\lambda/2H|_{\hat{t}+\Delta\hat{t}} - \hat{\omega}_m\lambda/2H|_{\hat{t}}$ and dividing both sides by $\Delta\hat{t}\Delta\hat{z_1}$ and tending $\Delta\hat{t}\Delta\hat{z_1}$ to zero gives

$$\frac{\partial Q}{\partial\hat{z}_1} = -\frac{\lambda}{2H}\frac{\partial\hat{\omega}_m}{\partial\hat{t}} \tag{28}$$

Substituting for Q by applying Eq. 26 to Eq. 28, the equation governing concentration is

$$\frac{\partial\hat{\omega}_m}{\partial\hat{t}} = \hat{K}\frac{\partial^2\hat{\omega}_m}{\partial\hat{z}_1^2} \tag{29}$$

Because of the fact that the average velocity variation in a horizontal cross section is zero and considering the effect of molecular diffusion in z-direction, the equation that needs to be solved is

$$\frac{\partial\hat{\omega}_m}{\partial\hat{t}} = \left(1+\hat{K}\right)\frac{\partial^2\hat{\omega}_m}{\partial\hat{z}^2} \tag{30}$$

by considering the following initial and boundary conditions

$$\hat{\omega}(\hat{z},0) = 0,\quad \hat{\omega}(0,\hat{t}) = 1,\quad \frac{\partial\hat{\omega}_m}{\partial\hat{z}}(1,\hat{t}) = 0 \tag{31}$$

The solution to Eq. 30 subjected to Eq. 31 can be obtained using the separation of variable method,[44] as given by

$$\hat{\omega}(\hat{z},\hat{t}) = 1 - \frac{4}{\pi}\sum_{n=1}^{\infty}\frac{1}{2n-1}\exp\left[-\frac{(2n-1)^2\pi^2}{4}\int_0^{\hat{t}}\left(1+\hat{K}\right)d\tau\right]\sin\left[\frac{(2n-1)\pi}{2}\hat{z}\right] \tag{32}$$

Although, Eq. 32 presents the concentration fields averaged in x-direction, it may not provide accurate concentration profile in z-direction. In other words, the 1-D model is only able to capture the average concentration because of the inherent dissimilarities between the Taylor's problem and our problem. As mentioned earlier, the intention of this study is the adaptation of the Taylor's theory of shear dispersion in combination with numerical simulations to derive a simple 1-D analytical model that characterizes the mixing process under steady and transient velocity fields.

The amount of passive tracer dissolved in the domain (i.e., convective mixing) can be obtained by a depth average of the concentration profile, which is expressed as

$$\hat{\bar{\omega}}(\hat{t}) = 1 - \frac{8}{\pi}\sum_{n=1}^{\infty}\frac{1}{(2n-1)^2}\exp\left[-\frac{(2n-1)^2\pi^2}{4}\int_0^{\hat{t}}\left(1+\hat{K}\right)d\tau\right] \tag{33}$$

where $\hat{K} = 0.5\delta(Ra\hat{v}_0/\hat{\alpha})^2$ in which $\hat{v_0}$ is either a constant (steady-state mixing) or a function of time (transient convective mixing).

The overall Sherwood number (Eq. 10) can be calculated by taking a derivative of the concentration profile (Eq. 33) at $\hat{z} = 0$

$$Sh(\hat{t}) = \left(1+\hat{K}\right)\frac{\sum_{n=1}^{\infty}\exp\left[-\frac{(2n-1)^2\pi^2}{4}\int_0^{\hat{t}}\left(1+\hat{K}\right)d\tau\right]}{\sum_{n=1}^{\infty}\exp\left[-\frac{(2n-1)^2\pi^2}{4}\hat{t}\right]} \tag{34}$$

Model Verification

In this section, the analytical model is validated with direct numerical solutions for both steady-state and transient

velocity fields. As the presented analytical solution (Eq. 33) can be used to evaluate convective mixing under both transient and steady-state conditions, different procedures need to be considered.

Steady-state velocity field

The classic steady-state convection in a porous layer of Horton-Rogers-Lapwood has been well studied in the literature.[37,45] In this study, a 2-D unicellular convection system is considered to simulate the steady-state convective mixing. In the steady-state convective regime, natural convection exists at Rayleigh numbers above the critical value of $4\pi^2$ ($Ra > 4\pi^2$). It has been shown that for a system with $Ra <$ 400 stable 2-D convection can exist, while above this value there are always unstable phenomena. Therefore, the analytical mixing model in this study refers physically to the stable convection that occurs at $Ra < 400$. However, the analytical model has been validated for Rayleigh numbers as high as 2000, by running the numerical simulations in sufficiently narrow and tall domains that house only one convection cell, $L/H < 1$. In other words, the slender domains straighten the flows, and the steady-state solutions persist in the Ra range 400–2000. Detailed information about steady-state unicellular convection is available in the literature.[46–48]

Numerical simulations were performed at different Rayleigh numbers (50, 100, 200, 400, 1000, and 2000), and the steady buoyancy-driven flows generated by thermal convection were characterized. To check and verify the accuracy of the numerical model, we compared the scaling relations obtained based on our numerical model with those reported in the literature for thermal natural convection. More details about numerical simulations and related scaling analyses have been presented elsewhere.[34]

In steady-state convection, the velocity of convection cells are independent of time; therefore, the dispersion coefficient is independent of time and the amount of tracer dissolved in the domain as a function of time (Eq. 33) can be expressed as

$$\hat{\bar{\omega}}(\hat{t}) = 1 - \frac{8}{\pi}\sum_{n=1}^{\infty}\frac{1}{(2n-1)^2}\exp\left[-\frac{(2n-1)^2\pi^2}{4}\left(1+\hat{K}\right)\hat{t}\right] \tag{35}$$

Direct numerical simulations are conducted to obtain the overall mixing when the domain is exposed to a constant concentration of a passive tracer from the top. The comparison between the numerical results and the results obtained from the developed model shows that the mixing process can be well described using the Taylor dispersion theory when $\delta =$ 0.0044. As the dimensionless velocity amplitude is constant and equal to 1 ($\hat{v}_0 = 1$) for a steady-state convective system, the dispersion coefficient for such system becomes

$$\hat{K} = 0.0022\left(\frac{Ra}{\hat{\alpha}}\right)^2 \tag{36}$$

where $\hat{\alpha} = \pi(H/L)$ in a unicellular convective system, and based on numerical results $H/L \approx 0.05Ra^{2/3}$ that provides the maximum or near maximum Nusselt number. The dispersion coefficient presented by Eq. 35 is identical to the dispersion coefficient obtained using a different approach in our previous study.[34]

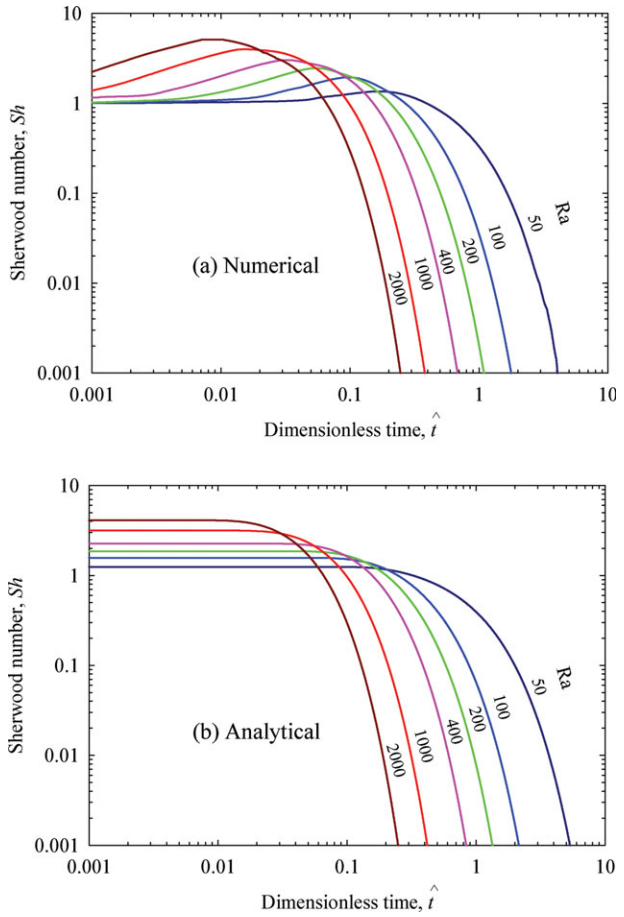

Figure 2. Sherwood number (*Sh*) vs. $\hat{t}$ at different *Ra* for the steady-state velocity field obtained from (a) the numerical simulations (Eqs. 3 and 10) and (b) the analytical calculations (Eqs. 34 and 36).

This results are similar to the results obtained in our previous study where different approach was used.[34] [Color figure can be viewed in the online issue, which is available at wileyonlinelibrary.com.]

Figure 2 shows the variation of the numerical (Figure 2a) and analytical (Figure 2b) Sherwood numbers as a measure of mixing efficiency vs. time for different Rayleigh numbers under the steady-state velocity field. Results show that the simple analytical model follows the same behavior at late time. However, the early time behavior is difficult to capture using a simple 1-D model due to the assumptions that have been made in development of the model and the condition given by Eq. 21, $Ra/\hat{\alpha}^2 << 57$.

Comparisons between numerical simulation and predicted results using the developed mixing model (Eq. 35) indicate a good accuracy for the 1-D mixing model with the dispersion coefficient given in Eq. 36 for Rayleigh numbers up to 2000. The results are shown in Figure 3, which is similar to the results obtained in our previous study based on analytically derived velocity fields.[34]

Transient velocity field

In the absence of a thermally driven flow field, the velocity field is coupled with the concentration field ($\beta_\omega > 0$). In this case, when the bottom of the porous layer is maintained at the zero mass flux condition (closed), the convective flow

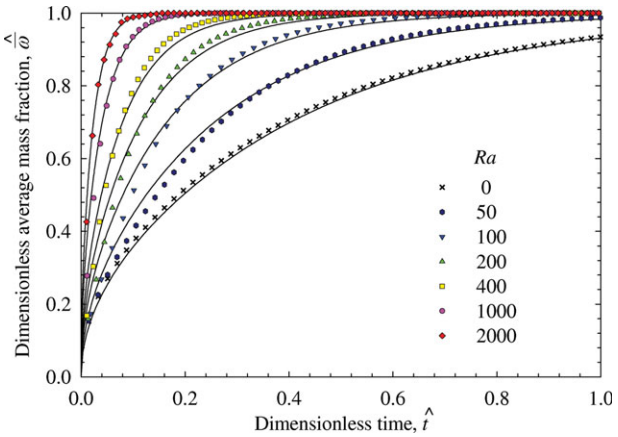

Figure 3. Mixing ($\hat{\bar{\omega}}$) vs. $\hat{t}$ at different *Ra* for a steady-state convection system.

Symbols are the results obtained from numerical simulations. Continuous lines are predictions of mixing ($\hat{\bar{\omega}}$) by the analytical model. This results are similar to the results obtained in our previous study where different approach was used.[34] [Color figure can be viewed in the online issue, which is available at wileyonlinelibrary.com.]

decays with time. Therefore, the amplitude of velocity varies with time, $\hat{v_0} = \hat{v_0}(\hat{t})$. As a result, the dispersion coefficient is expected to be time dependent. In this case, the dispersion coefficient is zero prior to the onset of convection, grows with time until it reaches a maximum, and then decays as the system becomes saturated with the matter. Direct numerical simulations are used to solve the transport equation (Eq. 4) coupled with the continuity equation (Eq. 1) and Darcy's law (Eq. 2) for flow in the porous layer. The resulting velocity field is then averaged using Reynolds' decomposition technique to find the effective dispersion coefficient for the governing velocity distribution[49]

$$\hat{K} = -Ra^2 \frac{H}{L} \int_0^{L/H} \hat{v}(\chi,\hat{t}) \int_0^{\hat{x}} \int_0^{\hat{x}} \hat{v}(\chi,\hat{t}) d\chi d\chi d\chi \tag{37}$$

The behavior of the vertical component of velocity ($\hat{v}$) across the domain (at $\hat{z} = 0.5$) for different periods of mixing time (for $Ra = 200$) is shown in Figure 4. As can be clearly seen from this Figure, the cosine behavior of $\hat{v}$ is consistent at different stages of mixing, and only the amplitude of the velocity rapidly grows with time, reaches a maximum, and then decays with time. The variation of the amplitude velocity ($\hat{v_0}$) and the effective dispersion with time for the problem of interest at the Rayleigh number of 200 are shown in Figure 5.

Considering the behavior of $\hat{v_0}$ and using the dispersion coefficient obtained based on the Taylor theory (Eq. 27) the dispersion coefficient $\hat{K}$ can be represented by a four-parameter Weibull function[50] as follows

$$\hat{K} = a\left(\frac{c-1}{c}\right)^{\frac{1-c}{c}} \left(\frac{\hat{t}-\hat{t}_0}{b} + \left(\frac{c-1}{c}\right)^{\frac{1}{c}}\right)^{c-1} \exp\left[\frac{c-1}{c} - \left(\frac{\hat{t}-\hat{t}_0}{b} + \left(\frac{c-1}{c}\right)^{\frac{1}{c}}\right)^{c}\right] \tag{38}$$

where a, b, c, and $\hat{t_0}$ are four parameters that need to be estimated from numerical simulations.

The effective dispersion coefficient is zero early in the process before the onset of natural convection ($\hat{t} < \hat{t_0} - b(1 - 1/c^{1/c})$ when the dominant mechanism is pure diffusion. Using the Weibull function to describe the time evolution of the dispersion coefficient for decaying convective mixing, the integral in Eq. 33 can be expressed by

$$\int_0^{\hat{t}} (1+\hat{K}) d\tau = \hat{t} + \frac{ab}{c}\left(\frac{c-1}{c}\right)^{\frac{1-c}{c}} \left(\exp\left[\frac{c-1}{c}\right] - \exp\left[\frac{c-1}{c} - \left(\frac{\hat{t}-\hat{t}_0}{b} + \left(\frac{c-1}{c}\right)^{\frac{1}{c}}\right)^{c}\right]\right) \tag{39}$$

The behaviors of parameters a, b, and c are obtained using the Monte Carlo simulation technique. The Monte Carlo simulation has been used successfully in many non-linear and complex problems for parameter estimation.[51] We used this technique to generate a large number of the physical problem realizations ($N = 10^6$) based on the deterministic model presented in this article (i.e., the analytical model for the transient case [Eqs. 33 and 39]). The procedure for implementing the Monte Carlo technique is as follows

1. Set a number of realizations or a Monte Carlo sampling (N),
2. Conduct a random sampling for each parameter and then generate input parameters (a, b, and c) for evaluating Eq. 39 using

$$a_i = a_{\min} + (a_{\max} - a_{\min})\xi_i \tag{40a}$$

$$b_i = b_{\min} + (b_{\max} - b_{\min})\xi_i \tag{40b}$$

$$c_i = c_{\min} + (c_{\max} - c_{\min})\xi_i \tag{40c}$$

where $\xi \in [0,1]$ is a random number sampled from a uniform distribution,

3. Obtain the average mixing analytically ($\hat{\bar{\omega}}_i^{\text{Ana}}$) using Eqs. 33 and 39,
4. Obtain the average mixing numerically ($\hat{\bar{\omega}}_i^{\text{Num}}$) using Eqs. 1–4,
5. Evaluate the objective function for this particular set of input,

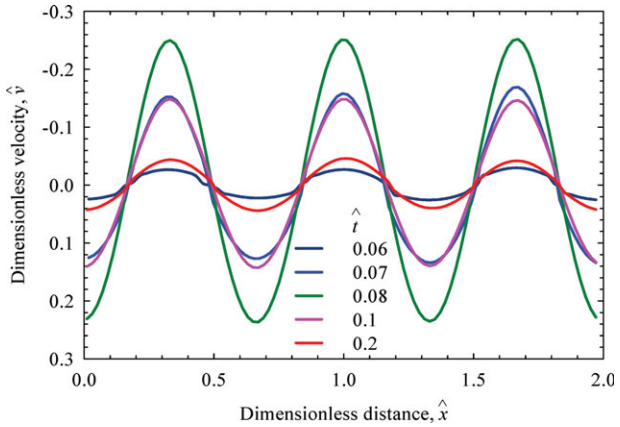

Figure 4. Numerical results for *Ra* = 200 at $\hat{z}$ = 0.5: Dimensionless vertical component of velocity ($\hat{v}$) as a function of $\hat{x}$ at different $\hat{t}$.

[Color figure can be viewed in the online issue, which is available at wileyonlinelibrary.com.]

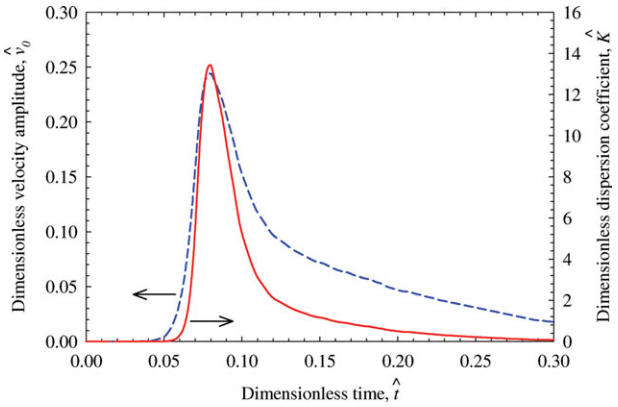

Figure 5. Dashed line (blue) shows $\hat{v}_0$ obtained from numerical simulation vs. $\hat{t}$, and the solid continuous line (red) shows the dispersion coefficient derived based on the Reynolds' decomposition method vs. $\hat{t}$, both at $Ra = 200$.

[Color figure can be viewed in the online issue, which is available at wileyonlinelibrary.com.]

$$\mathrm{SSE}_i = \sum_{i=1}^{n_t} \left(\hat{\bar{\omega}}_i^{\mathrm{Ana}} - \hat{\bar{\omega}}_i^{\mathrm{Num}} \right)^2 \tag{41}$$

where SSE is the Sum Square of Errors, n_t is the number of events, and the superscripts Ana and Num denote the analytical and numerical values, respectively.

6. Repeat steps 2 to 5 for N times,

7. Analyze the results from all accepted realizations and locate the input set that minimizes the objective function.

The numerical results obtained from Monte Carlo simulations suggest that parameter a scales linearly with time, while parameters b and c are decreasing functions of the Rayleigh number.

From the Weibull function and the behavior of the dispersion (Eq. 38), one would expect that $1 < c < 2$. This suggests that $c \to 1$ as $Ra \to \infty$ and $c \to 2$ as $Ra \to 0$. Thus, the relation between c and Ra may be expressed by $c = 1 + \exp[-c_1 Ra]$, where c_1 is constant. Parameter a plays the amplitude role of the dimensionless dispersion coefficient and scales linearly with Ra, while parameter b decreases with the Rayleigh number. Using Monte Carlo simulations and regression analysis, the following relationships were derived for a, b, and c as a function of the Rayleigh number and can be expressed as

$$a = a_1 + a_2\, Ra, \text{ where } a_1 = -0.8 \text{ and } a_2 = 0.014 \tag{42}$$

$$b = b_1 - b_2\, Ra, \text{ where } b_1 = 0.1765 \text{ and } b_2 = 0.0001 \tag{43}$$

$$c = 1 + \exp[-c_1 Ra] \text{ where } c_1 = 0.008 \tag{44}$$

The fourth parameter ($\hat{t}_0$) is the dimensionless time corresponding to the maximum Sherwood number or dimensionless flux. The behavior of this parameter vs. Ra obtained from numerical simulations is shown in Figure 6. As the bottom boundary has not been affected at this time, it is expected that this time will be independent of the porous layer thickness. It is evident that the dimensionless time at the maximum flux scales with $1/Ra^2$, implying that the dimensional time is independent of the porous layer thickness,

$$\hat{t}_0 = \frac{3800}{Ra^2} \tag{45}$$

During a pure diffusive mixing process $\hat{K} = 0$ for $\hat{t} < \hat{t}_0 - b(1-1/c)^{1/c}$. In other words, at $\hat{t}_c = \hat{t}_0 - b(1 - 1/c)^{1/c}$, the diffusive boundary layer becomes unstable, which is considered as the onset of convection. Using Eqs. 42–45, the critical dimensionless time can be expressed by

$$\hat{t}_c = \frac{2700}{Ra^2} \tag{46}$$

As the critical dimensionless time is inversely proportional to the porous layer thickness to the power of two and the Rayleigh number is proportional to the layer thickness, the dimensional time to the onset of convection is, therefore, independent of the porous layer thickness. This scaling behavior is similar with results obtained from direct numerical simulations and a linear stability analysis;[52,53] however, the coefficient (2700 in Eq. 46) is larger than the reported value in the literature (500).[42] This is due to the fact that, in this study, $\hat{t}_c$ is defined as the time at which the convective mixing curve departs from the diffusive one; whereas, in the analysis presented by Hassanzadeh et al.,[42] the onset was defined as the time at which the diffusive boundary layer starts to deform.

The behavior of the derived effective dispersion for different Rayleigh numbers is analyzed and depicted in Figure 7. The loci of maximums correspond to the time at the maximum Sherwood number and scales with $1/Ra^2$.

Figure 8 shows the calculated concentration distribution (Figure 8a) with the corresponding velocity vectors (Figure 8b) at $\hat{t}_0$ for Ra, 150, 200, 300, 400, and 500. At small Rayleigh numbers, there are only a few fingers penetrating downward with no interaction with each other; whereas, at higher Rayleigh numbers, more fingers are generated, and their interactions retard their free movements toward the bottom boundary. In other words, the wavelength is smaller for higher Rayleigh numbers, resulting in the generation of a stronger convection current earlier in the mixing process. Moreover, at small Rayleigh numbers, the velocity fields are weaker than those at higher Rayleigh numbers.

Figure 9 shows the variation of the numerical and analytical Sherwood numbers (Figure 9a and Figure 9b, respectively) as

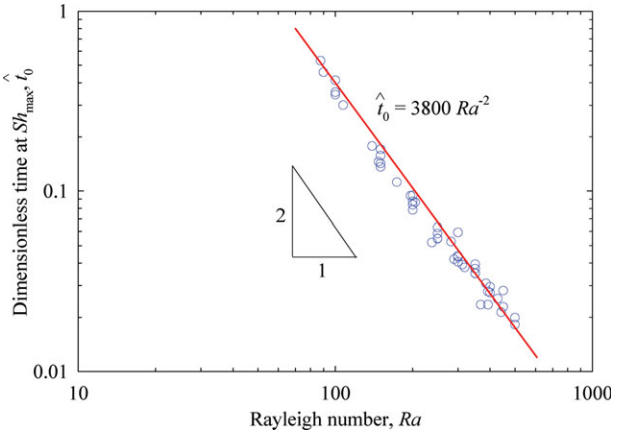

Figure 6. Dimensionless time at the maximum Sherwood number ($\hat{t}_0$) obtained from numerical simulations vs. Ra.

[Color figure can be viewed in the online issue, which is available at wileyonlinelibrary.com.]

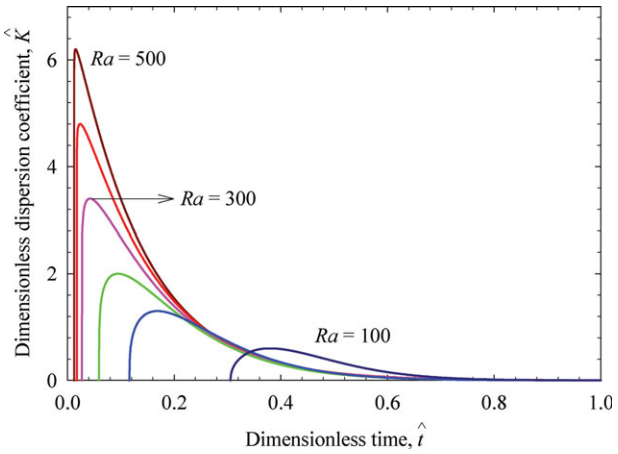

Figure 7. Dimensionless dispersion coefficient ($\hat{K}$) calculated based on the analytical model vs. $\hat{t}$ at *Ra* = 100, 150, 200, 300, 400, and 500.

[Color figure can be viewed in the online issue, which is available at wileyonlinelibrary.com.]

a measure of mixing efficiency vs. time with different Rayleigh numbers for the transient convection systems. Results show that the simple analytical model was able to reproduce the late time behavior of the mixing process as compared with the numerical simulations. While numerical and analytical results at low Rayleigh numbers are more accurate, the early time predictions deviate from the numerical simulations as the Rayleigh number increases. This is due to the underlying assumptions have been made in development of the simple 1-D model ($Ra\hat{v}_0/\hat{\alpha}^2 << 57$). It can readily be seen from Figure 9a, as the Rayleigh number increases the value at the peak of the Sherwood number curve increases. This fact originates from the non-linear interaction between fingers shown in Figure 8, which cannot be captured by the simple 1-D mixing model.

The rate of mixing obtained from the analytical model (Eq. 33) vs. the Rayleigh number shortly after the evolution of the instabilities (i.e., $\hat{t_c} = \hat{t_0} - (1-\varepsilon)b(1-1/c)^{1/c}$ where $\varepsilon = 0.05$) is shown by scaling in Figure 10a. The results indicate that the dimensionless rate of mixing scales with the Rayleigh number, which is characteristic of the early behavior of convective mixing. These analytical results follow similar scaling behavior when compared with direct numerical simulations of convective mixing,[42,54] which is an indication of a pure convective instability.

Figure 10b shows the rate of mixing ($d\hat{\bar{\omega}}/d\hat{t}$) vs. dimensionless time obtained from the analytical mixing model (Eqs. 33 and 39). Three mixing regimes can be clearly identified. The first regime is the pure diffusive mixing early in the process, where $d\hat{\bar{\omega}}/d\hat{t}$ scales with $1/\sqrt{\hat{t}}$, implying $\hat{\bar{\omega}}$ scales with $\sqrt{\hat{t}}$. This scaling indicates that the system is saturating with the diffusing species with $\sqrt{\hat{t}}$.

The second regime can be observed for large Rayleigh numbers after the onset of convection, where $d\hat{\bar{\omega}}/d\hat{t}$ varies with $1/\hat{t}^2$, implying $\hat{\bar{\omega}}$ scales with $\ln[\hat{t}]$. However, for small Rayleigh numbers, the system is boundary dominated, and the second regime cannot be observed.

The third regime is a mixing period, where $d\hat{\bar{\omega}}/d\hat{t}$ nearly scales with $1/\hat{t}^2$, implying a weak mixing regime where $\hat{\bar{\omega}}$ is proportional to $1/\hat{t}$.

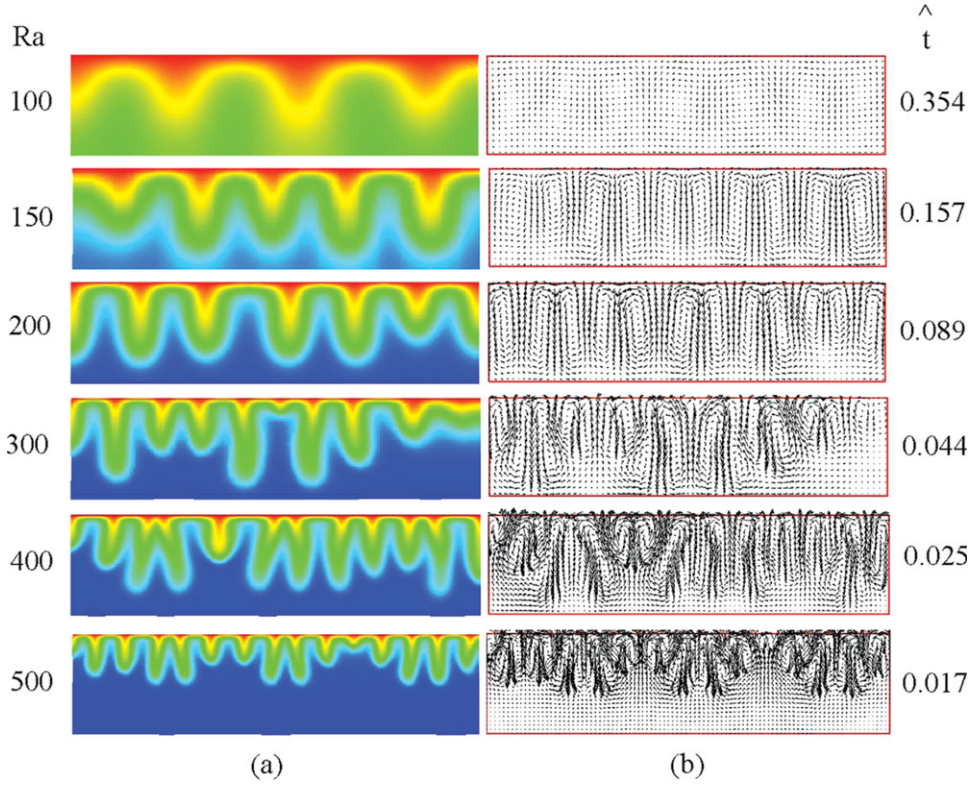

Figure 8. Numerical results at $\hat{t}_0$ for *Ra* = 100, 150, 200, 300, 400, and 500.

(a) Snapshots of concentrations, where red and blue colors mean $\hat{\omega} = 1$ and $\hat{\omega} = 0$, respectively, and (b) the corresponding velocity vectors. [Color figure can be viewed in the online issue, which is available at wileyonlinelibrary. com.]

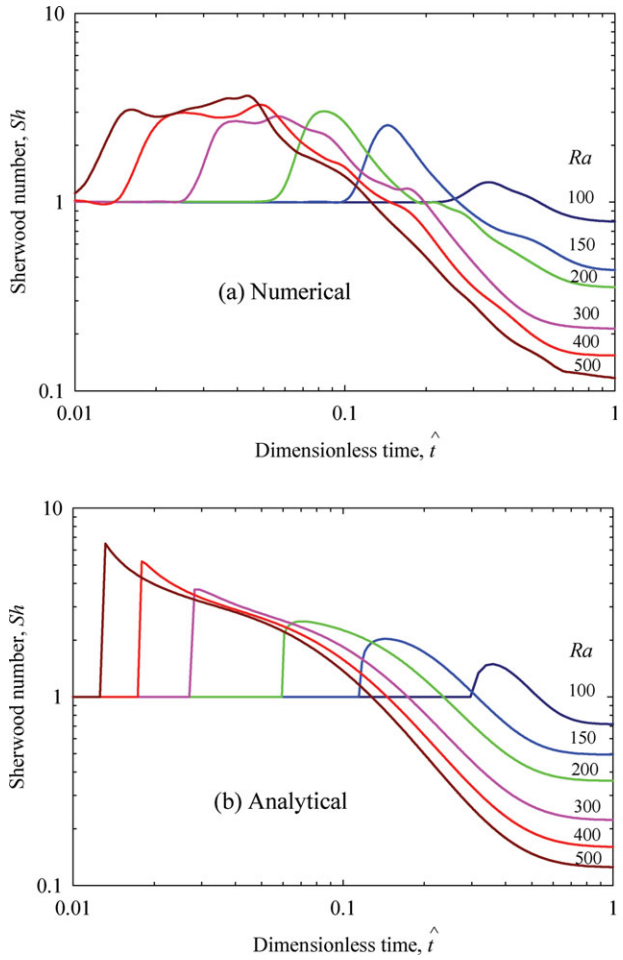

Figure 9. Sherwood number (*Sh*) vs. $\hat{t}$ at different *Ra* for the transient convection systems obtained from (a) the numerical simulations (Eqs. 3 and 10) and (b) the analytical calculations (Eqs. 34, 38, and 39).

[Color figure can be viewed in the online issue, which is available at wileyonlinelibrary.com.]

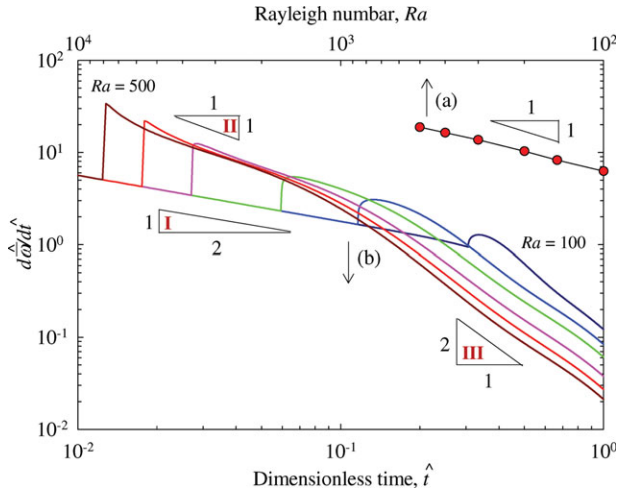

Figure 10. (a) Rate of mixing vs. *Ra*, confirming that the rate of mixing is proportional to *Ra*.

(b) Rate of mixing vs. $\hat{t}$ for three mixing regimes at different *Ra*. [Color figure can be viewed in the online issue, which is available at wileyonlinelibrary.com.]

In the case of steady-state buoyancy-driven flow, the velocity and concentration fields were decoupled to allow the study of the mixing process in a time-independent velocity field. In this method, convection cells are generated by thermal convection. After the convection cells reached the steady-state condition, a passive tracer was introduced at the top of the domain; and, the mixing due to such a flow behavior was studied. Comparisons between numerical results and analytical predictions demonstrated good agreement for the unicellular convection with Rayleigh numbers up to 2000. These results are similar to the results obtained in our previous study,[34] where different approach was used.

In the transient case, the convective flow decays with time; consequently, the dispersion coefficient demonstrates a time-dependent behavior. It was shown that this behavior can be characterized by a four-parameter Weibull function. The analytical solution obtained was then compared with the

The comparisons between the numerical solution and the 1-D analytical solution obtained based on the Taylor dispersion theory (Eqs. 33, 39, and 41–45) for different Rayleigh numbers is shown in Figure 11. Results show that the analytical model is able to adequately predict the mixing behavior. Once the effect of the bottom boundary turns out to be dominant, the density gradients diminish; consequently, the convection cells gradually die down.

Conclusion

We have studied the mixing of a passive tracer in steady and transient flow fields at different Rayleigh numbers. A simple 1-D analytical model based on the Taylor dispersion theory has been developed to characterize the dynamics of steady and transient buoyancy-driven flows. It has been shown that the analytical model accurately predicts steady-state and transient convective mixing obtained from high-resolution numerical simulations. We found that the buoyancy-driven mixing process can be well described by the framework of the Taylor dispersion theory using a simple modification.

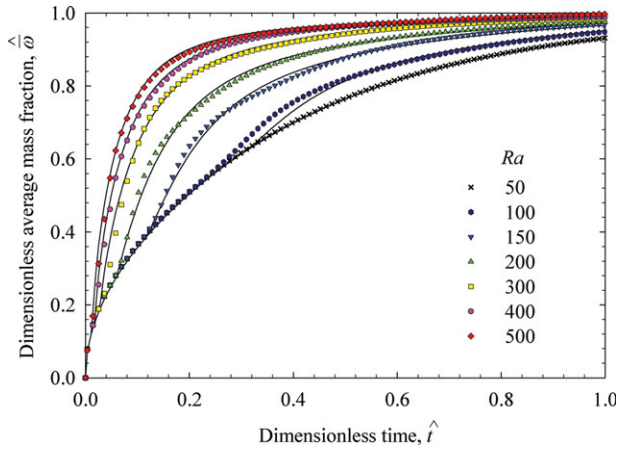

Figure 11. Mixing ($\hat{\bar{\omega}}$) vs. $\hat{t}$ at different *Ra* for a transient convection system.

Symbols are the results obtained from numerical simulations. Continuous lines are predictions of mixing by the analytical model. [Color figure can be viewed in the online issue, which is available at wileyonlinelibrary.com.]

numerical solutions for a laminar convective system with Rayleigh numbers less than 500, showing good agreement. In addition, the 1-D analytical mixing model was able to identify three mixing regimes during the mixing process.

Scaling relations have been reported in the literature to characterize buoyancy-driven mixing. Such scaling relations have been obtained using high-resolution numerical simulations or experimental observations. It was shown that the simple analytical model developed in this work can recover scaling relations reported in the literature and can be used to characterize the mixing process in transient buoyancy-driven flows.

In this study, we have investigated buoyancy-driven induced mixing at low Rayleigh numbers. At high Rayleigh numbers, turbulent flow may lead to strong nonlinear interactions between density-driven instabilities, such as merging and splitting of fingers; and this phenomenon needs further investigations.

Acknowledgments

The authors would like to thank M. Pooladi-Darvish at the University of Calgary for many fruitful discussions. This research has been enabled with financial support from the Natural Sciences and Engineering Research Council of Canada (NSERC) and the Department of Chemical and Petroleum Engineering at the University of Calgary, and with the use of computing resources provided by WestGrid and Compute Canada.

Notation

A = dimensionless cross section area, –
a,b,c = Weibull function parameters, –
c = specific heat capacity, J/kg/K
D = molecular diffusion coefficient, m^2/s
$\mathbf{e}_z$ = unit vector in z-direction,–
g = gravity acceleration, m/s^2
H = thickness of porous layer, m
k = permeability, m^2
K = dispersion coefficient, m^2/s
L = length of porous layer, m
N = Monte Carlo sampling number, –
n_t = number of events, –
Nu = overall Nusselt number, –
Pe_j = grid Peclet number, –
Q = dimensionless rate of mass transfer, –
R = radius, m
Ra = overall Rayleigh number, –
Ra_j = grid Rayleigh number, –
Sh = overall Sherwood number, –
SSE = sum square of errors, –
t = time, s
t_0 = time at maximum Sherwood number, s
t_c = critical time, s
T = temperature, K
T_0 = temperature density at $z = 0$, K
T_1 = temperature density at $z = H$, K
u = horizontal component of velocity, m/s
v = vertical component of velocity, m/s
v_0 = amplitude of the vertical component of velocity, m/s
$\mathbf{v}$ = velocity vector, m/s
V = mean velocity, m/s
w = a constant number, –

Greek letters

α = thermal diffusivity, m^2/s
α = wave number, 1/m
β = expansion coefficient, 1/K or m^3/kg
γ = eigenvalue, –
δ = correction factor, –
ε = constant small number, –
Δl = grid block size, m
$\Delta\rho$ = density difference, kg/m^3
κ = thermal conductivity, W/m/K
λ = wavelength, m
μ = viscosity, Pa.s
ξ = random number, –
ρ = density, kg/m^3
ρ_0 = density at $t = 0$, kg/m^3
σ = heat capacity ratio, –
τ = dummy variable of integration for time, –
ϕ = porosity, –
χ = dummy variable of integration for x-direction,–
ω = mass fraction, kg/m^3
ω_0 = mass fraction at $z = 0$, kg/m^3

Other symbols

$(\hat{})$ = dimensionless variables
$()^{\mathrm{Ana}}$ = analytical
$()_{\mathrm{Cond}}$ = conduction
$()_{\mathrm{Conv}}$ = convection
$()_{\mathrm{Diff}}$ = diffusion
$()_{\mathrm{f}}$ = fluid phase
$()_{\mathrm{m}}$ = mean
$()_{\mathrm{min}}$ = minimum
$()_{\mathrm{max}}$ = maximum
$()^{\mathrm{Num}}$ = numerical
$()_{\mathrm{s}}$ = solid phase
$()_T$, $()^T$ = thermal
$()_\omega$, $()^\omega$ = solutal

Literature Cited

1. Marotzke J, Scott JR. Convective mixing and the thermohaline circulation. *J Phys Oceanogr*. 1999;29:2962–2970.
2. Trompert R, Hansen U. Mantle convection simulations with rheologies that generate plate-like behaviour. *Nature*. 1998;395:686–689.
3. Smith AJ. Mixed convection and density-dependent seawater circulation in coastal aquifers. *Water Resour Res*. 2004;40:W08309.
4. Ghesmat K, Hassanzadeh H, Abedi J. The impact of geochemistry on convective mixing in a gravitationally unstable diffusive boundary layer in porous media: CO_2 storage in saline aquifers. *J Fluids Mech*. 2011;673:480–512.
5. Neufeld JA, Hesse MA, Riaz A, Hallworth MA, Tchelepi HA, Huppert HE. Convective dissolution of carbon dioxide in saline aquifers. *Geophys Res Lett*. 2010;37:L22404.
6. Diersch HJG, Kolditz O. Variable-density flow and transport in porous media: approaches and challenges. *Adv Water Res*. 2002;25:899–944.
7. Bérnard H. Les tourbillons cellulaires dans une nappe liquide transportant de la chaleur par convection en regime permanent. *Ann Chim Phys*. 1901;23:62–144.
8. Rayleigh L. On convection currents in a horizontal layer of fluid when the higher temperature is on the other side. *Philos Mag*. 1916;32:529–543.
9. Horton C, Rogers F. Convection currents in a porous medium. *J Appl Phys*. 1945;16:367–370.
10. Lapwood ER. Convection of a fluid in a porous medium. *Math Proc Cambridge Philos Soc*. 1948;44:508–521.
11. Schmalzl J, Hansen U. Mixing the earth's mantle by thermal convection: a scale dependent phenomenon. *Geophys Res Lett*. 1994;21:987–987.
12. Brenner H, Edwards DA. *Macrotransport Processes*. Stoneham, MA: Butterworth-Heinemann, 1993.
13. Taylor G. Dispersion of soluble matter in solvent flowing slowly through a tube. *Proc R Soc London Ser A*. 1953;219:186–203.
14. Taylor G. The dispersion of matter in turbulent flow through a pipe. *Proc R Soc London Ser A*. 1954;223:446.
15. Aris R. On the dispersion of a solute in a fluid flowing through a tube. *Proc R Soc London Ser A*. 1956;235:67–77.
16. Aris R, Amundson NR. Some remarks on longitudinal mixing or diffusion in fixed beds. *AlChE J*. 1957;3:280–282.
17. Aris R. On the dispersion of a solute in pulsating flow through a tube. *Proc R Soc London Ser A*. 1960:370–376.
18. Horn F. Calculation of dispersion coefficients by means of moments. *AlChE J*. 1971;17:613–620.
19. Brenner H. A general theory of Taylor dispersion phenomena. *PhysicoChem Hydrodyn*. 1980;1:91–123.
20. Brenner H. A general theory of Taylor dispersion phenomena IV. Direct coupling effects. *Chem Eng Commun*. 1982;18:355–379.

21. Brenner H. General theory of Taylor dispersion phenomena. II. An extension. *Physcochem Hydrodyn.* 1982;3:139–157.
22. Young W, Jones S. Shear dispersion. *Phys Fluids A.* 1991;3:1087.
23. Woods AW, Linz SJ. Natural convection and dispersion in a tilted fracture. *J Fluids Mech.* 1992;241:59–74.
24. Linz SJ, Woods AW. Natural convection, Taylor dispersion, and diagenesis in a tilted porous layer. *Phys Rev A.* 1992;46:4869.
25. Brenner H, Adler P. Dispersion resulting from flow through spatially periodic porous media II. Surface and intraparticle transport. *Philos Trans R Soc London Ser A.* 1982;307:149–200.
26. Koch DL, Cox RG, Brenner H, Brady JF. The effect of order on dispersion in porous media. *J Fluids Mech.* 1989;200:173–188.
27. Eckmann DM, Grotberg JB. Oscillatory flow and mass transport in a curved tube. *J Fluids Mech.* 1988;188:527.
28. Camacho J. Purely global model for Taylor dispersion. *Phys Rev E Stat Phys Plasmas Fluids Relat Interdiscip Topics.* 1993;48:310.
29. Codd S, Manz B, Seymour J, Callaghan P. Taylor dispersion and molecular displacements in Poiseuille flow. *Phys Rev E Stat Phys Plasmas Fluids Relat Interdiscip Topics.* 1999;60:3491–3494.
30. Dorfman KD, Brenner H. Generalized Taylor-Aris dispersion in discrete spatially periodic networks: microfluidic applications. *Phys Rev E Stat Nonlin Soft Matter Phys.* 2002;65:021103.
31. Jansons KM. On Taylor dispersion in oscillatory channel flows. *Proc R Soc Ser A.* 2006;462:3501.
32. Biswas RR, Sen PN. Taylor dispersion with absorbing boundaries: a stochastic approach. *Phys Rev Lett* 2007;98:164501.
33. Giona M, Cerbelli S. Perturbation analysis of mixing and dispersion regimes in the low and intermediate Péclet number region. *Phys Rev E.* 2010;81:046309.
34. Emami Meybodi H, Hassanzadeh H. Hydrodynamic dispersion in steady buoyancy-driven geological flows. *Water Resour Res.* 2011;47:W12504.
35. Chandrasekhar S. *Hydrodynamic and Hydromagnetic Stability*. New York: Oxford University Press, 1961.
36. Bear J. *Dynamics of Fluids in Porous Media*. New York: Dover Publications, 1988.
37. Nield DA, Bejan A. *Convection in Porous Media*. New York: Springer Verlag, 2006.
38. Kolditz O, Ratke R, Diersch HJG, Zielke W. Coupled groundwater flow and transport: 1. Verification of variable density flow and transport models. *Adv Water Res.* 1998;21:27–46.
39. Ibaraki M. A robust and efficient numerical model for analyses of density-dependent flow in porous media. *J Contam Hydrol.* 1998;34:235–246.
40. Burnett RD, Frind EO. Simulation of contaminant transport in three dimensions: 1. The alternating direction Galerkin Technique. *Water Resour Res.* 1987;23:683–694.
41. Burnett R, Frind E. Simulation of contaminant transport in three dimensions: 2. Dimensionality effects. *Water Resour Res.* 1987;23:695–705.
42. Hassanzadeh H, Pooladi-Darvish M, Keith DW. Scaling behavior of convective mixing, with application to geological storage of CO_2. *AlChE J.* 2007;53:1121–1131.
43. Trevisan OV, Bejan A. Mass and heat transfer by high Rayleigh number convection in a porous medium heated from below. *Int J Heat Mass Transfer.* 1987;30:2341–2356.
44. Ozisik MN. *Heat Conduction*, New York: Wiley, 1993.
45. Kaviany M. *Principles of Convective Heat Transfer*. New York: Springer Verlag, 2001.
46. Caltagirone J. Thermoconvective instabilities in a horizontal porous layer. *J Fluids Mech.* 1975;72(pt 2):267–287.
47. Robinson J, O'sullivan M. A boundary-layer model of flow in a porous medium at high Rayleigh number. *J Fluids Mech.* 1976;75:459–467.
48. Kimura S, Schubert G, Straus J. Route to chaos in porous-medium thermal convection. *J Fluids Mech.* 1986;166:305–324.
49. Fischer HB. *Mixing in Inland and Coastal Waters*. San Diego, CA: Academic Press, 1979.
50. Kasnavi A, Wang JW, Shahram M, Zejda J. Analytical modeling of crosstalk noise waveforms using Weibull function. In: International conference on Computer-aided design, San Jose, CA, 2004.
51. Aggarwal M, Carrayrou J. Parameter estimation for reactive transport by a Monte-Carlo approach. *AlChE J.* 2006;52:2281–2289.
52. Ennis-King J, Preston I, Paterson L. Onset of convection in anisotropic porous media subject to a rapid change in boundary conditions. *Phys Fluids.* 2005;17:084107.
53. Riaz A, Hesse M, Tchelepi H, Orr F. Onset of convection in a gravitationally unstable diffusive boundary layer in porous media. *J Fluids Mech.* 2006;548:87–111.
54. Howard LN. *Convection at high Rayleigh number*. In: *Eleventh International Congress Applied Mechanics*, Munich, 1966.

Manuscript received Jan. 15, 2012, and revision received July 10, 2012.